DOI: 10.1002/anie.201201991

Nanotube Toxicology

Degree of Chemical Functionalization of Carbon Nanotubes Determines Tissue Distribution and Excretion Profile**

Khuloud T. Al-Jamal, Antonio Nunes, Laura Methven, Hanene Ali-Boucetta, Shouping Li, Francesca M. Toma, M. Antonia Herrero, Wafa' T. Al-Jamal, Huub M. M. ten Eikelder, Julie Foster, Stephen Mather, Maurizio Prato, Alberto Bianco,* and Kostas Kostarelos**

Carbon nanotubes (CNTs) were first described at the atomic level by Iijima in the 1990s.[1] Pristine (as-produced, non-functionalized) CNTs are water insoluble and a variety of chemical strategies have been explored to functionalize the nanotube surface and make them dispersible in aqueous environments.[2–5] Some years ago we reported the functionalization by 1,3-dipolar cycloaddition of azomethine ylides onto the carbon backbone of the tubes to append hydrophilic amino groups to the inherently hydrophobic carbon structure.[6] To understand the pharmacokinetic profile of CNTs chemically modified by addition reactions, we have previously evaluated the biodistribution of functionalized single-walled (*f*-SWNTs) and multi-walled (*f*-MWNTs) CNTs after intravenous administration in mouse and rat models.[7,8] Ammonium *f*-SWNTs (average diameter of 1 nm; average length of 300–1000 nm)[7] and *f*-MWNTs (average diameter of 20–30 nm; average length of 500–2000 nm)[8] were conjugated with the chelating molecule diethylentriaminepentaacetic dianhydride (DTPA) and then labeled with radioactive indium (^{111}In) for tracking purposes.

Previous dynamic imaging studies by SPECT/CT (single-photon emission computed tomography) and quantitative gamma scintigraphy indicated rapid clearance of highly functionalized nanotubes from systemic blood circulation through renal excretion with minimal accumulation in the reticuloendothelial system (RES). Subsequent studies verified independently this behavior by showing rapid clearance of short hydroxylated SWNTs[9] or ammonium *f*-SWNTs[10] after intravenous administration in mice. Renal clearance of carboxylated glucosamine *f*-MWNTs was also reported after intraperitoneal administration.[11] Contrary to the above mentioned studies, other work has shown accumulation of macromolecule (polymer or lipopolymer)-coated MWNTs accumulating mainly in RES organs, such as liver and spleen.[12,13] We have also reported liver and lung accumulation of serum-coated, non-functionalized MWNTs.[14]

Several factors are believed to play a role in the in vivo fate of CNTs including the type of surface modification (physical coating versus chemical functionalization) and the degree of chemical functionalization.[15] Since pharmacokinetic profiling of carbon-based nanomaterials is essential for both pharmacological and toxicological reasons, this study attempts to determine the effect of the degree of MWNT chemical functionalization on their ensuing pharmacokinetic profile. Two strategies were used to functionalize MWNTs with DTPA molecules (Scheme 1). In the first strategy, ammonium *f*-MWNTs were prepared by 1,3-dipolar cycloaddition and subsequently conjugated to DTPA as previously reported.[8] In the second approach, MWNTs were first oxidized by acid treatment, followed by amidation and conjugation to DTPA.[16]

The oxidation of carbon nanotubes by strong acids, along with sonication, shortened the carbon nanotubes and introduced carboxylate groups, mostly at the tube tips and the defect sites. The carboxylate groups were then converted by an amidation reaction generating *f*-MWNTs with several amino groups, which were subsequently conjugated to DTPA. The derived DTPA-MWNTs (MWNTs **6**, **7**, and **8**) were then chelated with radioactive ^{111}In. Based on the degree of chemical functionalization, the DTPA-MWNTs studied were categorized into two types: those with a low degree of functionalization (modified by 1,3-dipolar cycloaddition or

[*] Dr. K. T. Al-Jamal,[+] Dr. A. Nunes,[+] Dr. L. Methven, Dr. H. Ali-Boucetta, Dr. W. T. Al-Jamal, Prof. K. Kostarelos
Nanomedicine Laboratory, Centre for Drug Delivery Research, UCL School of Pharmacy, University College London
London WC1N 1AX (UK)
E-mail: k.kostarelos@ucl.ac.uk

Dr. S. Li, Dr. A. Bianco
CNRS, Institut de Biologie Moléculaire et Cellulaire, Laboratoire d'Immunologie et Chimie Thérapeutiques
67000 Strasbourg (France)
E-mail: a.bianco@ibmc-cnrs.unistra.fr

Dr. F. M. Toma, Dr. M. A. Herrero, Prof. M. Prato
Dipartimento di Scienze Farmaceutiche, Università di Trieste
34127 Trieste (Italy)
E-mail: prato@units.it

Dr. H. M. M. ten Eikelder
Biomodeling and Bioinformatics Group, Eindhoven University of Technology (The Netherlands)

Dr. J. Foster, Prof. S. J. Mather
Department of Nuclear Medicine, St Bartholomew's and The London Hospital (UK)

[+] These authors contributed equally to this work.

[**] This work was partially supported by the Engineering and Physical Sciences Research Council (EPSRC) Grand Challenge grant (EP/G061998/1) and the European Commission FP7 ANTICARB (HEALTH-2007-201587), and CARBONANOBRIDGE (ERC-2008-AdG-227135) programs. M.P. acknowledges the University of Trieste, INSTM, Italian Ministry of Education MUR (Cofin Prot. 20085M27SS and Firb RBAP11ETKA), Regione Friuli Venezia-Giulia, and A.B. the CNRS and the Agence Nationale de la Recherche (grant ANR-05-JCJC-0031-01). Also, A.B. acknowledges the PICS (Project for International Scientific Cooperation) CNRS financial support.

Supporting information for this article is available on the WWW under http://dx.doi.org/10.1002/anie.201201991.

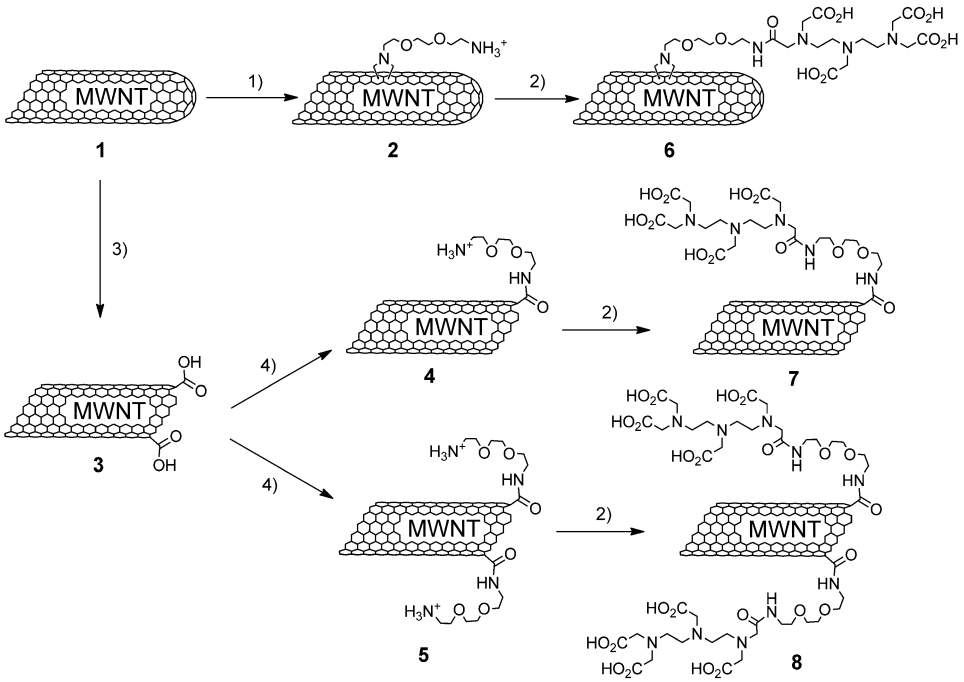

Scheme 1. Synthesis of the different DTPA-MWNTs. 1) 1. Boc-NH-$(CH_2CH_2O)_2$-CH_2CH_2-NH-CH_2-COOH/$(H_2CO)_n$ in dimethylformamide (DMF); 2. 4 M HCl in dioxane. 2) *N*,*N*-diisopropylethylamine/DTPA in dry DMSO/DMF. 3) H_2SO_4/HNO_3 (3:1), sonication. 4) 1. Neat $(COCl)_2$; 2. Boc-NH-$(CH_2CH_2O)_2$-CH_2CH_2-NH_2, dry tetrahydrofuran; 3. 4 M HCl in dioxane. Boc = *tert*-butyloxycarbonyl.

amidation reaction), corresponding to 0.058–0.115 mmol of amino groups per gram of nanotube material (MWNTs **6** and **7**), and those of an intermediate degree of functionalization, corresponding to 0.320 mmol g^{-1} (MWNT **8**). The quantitative Kaiser test was used to determine the amount of free amino groups before and after DTPA loading. The characteristics, in terms of functional groups, of the DTPA-MWNTs are summarized in Table S1 (see Supporting Information).

Transmission electron microscopy (TEM) images of the DTPA-MWNT constructs were obtained after aqueous dispersion, deposition onto a TEM grid, and evaporation of water (Figure 1). Using Image J analysis of TEM micrographs, we measured the diameter average of the pristine nanotubes and the length distribution of both non-oxidized MWNTs used for the preparation of DTPA-MWNT **6** and oxidized MWNTs used for the synthesis of DTPA-MWNT **7** and **8** (Supporting Information, Figure S1). The diameter distribution of the nanotubes was not affected during the chemical treatment and indicated an average diameter of 34.1 nm (± 10.2 nm). Determination of the length distribution yielded a mean (± SD, standard deviation) of 773 nm (± 425 nm) for the nanotube precursors of MWNT **6** and 354 nm (± 170 nm) for the shortened nanotubes used in the preparation of MWNTs **7** and **8**.

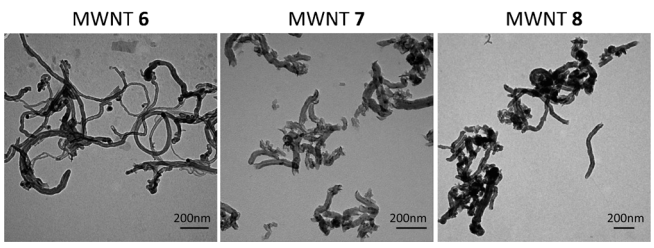

Figure 1. Morphological characterization of *f*-MWNTs. Representative TEM images of the DTPA-MWNTs dispersed in water. Scale bar = 200 nm.

To perform in vivo imaging of the DTPA-MWNT constructs in mice, the material was radiolabeled with ^{111}In, which was chosen because of its half-life (67.5 h) and because the chelating agent DTPA rapidly cages ^{111}In with a high thermodynamic equilibrium constant.[17] DTPA-MWNTs were radiolabeled as described in the Supporting Information. The reaction efficiency was determined by thin layer chromatography (TLC) and phosphorimaging. Quenched ^{111}In-EDTA (ethylenediaminetetraacetic acid) migrated to the solvent front while ^{111}In-DTPA-MWNTs remained at the application point (Supporting Information, Figure S2 and Table S2). As expected, the specific radioactivity (MBq/mg of CNTs) increased as the degree of chemical functionalization and DTPA loading increased. The excess of residual ^{111}In was quenched by addition of EDTA, and then removed by centrifugation. ^{111}In-DTPA-MWNT pellets were recovered and resuspended in 5% dextrose before administration into mice. The absence of free ^{111}In in the injected dose was confirmed by TLC analysis of the "ready to inject" material. Serum stability studies were conducted by assessing the free ^{111}In released in the dispersion after 24 h incubation in 50% mouse serum at 37 °C (Supporting Information, Figure S3). All radiolabeled constructs showed the same good stability in the presence of serum before injection.

Each group of animals ($n = 4$) was injected in the tail vein with 50 μg of ^{111}In-DTPA-MWNT containing approximately 5–6 MBq. Three-dimensional reconstruction of whole-body images by SPECT/CT of ^{111}In-DTPA-MWNTs or ^{111}In-EDTA was conducted at 0.5, 3.5, and 24 h after injection of the radiolabeled complex. SPECT/CT imaging of MWNT **6** showed accumulation predominantly in the liver followed by the spleen, then the lung (Figure 2). Signals were also detected in the bladder at an early time point (0.5 h), which is due to early excretion of the individualized MWNT fraction. SPECT/CT imaging of MWNT **7** showed a similar profile as MWNT **6** at all time points. MWNT **8** exhibited an altered organ distribution profile compared to MWNTs **6** and **7** with a clear reduction in liver accumulation. Moreover, at 0.5 h

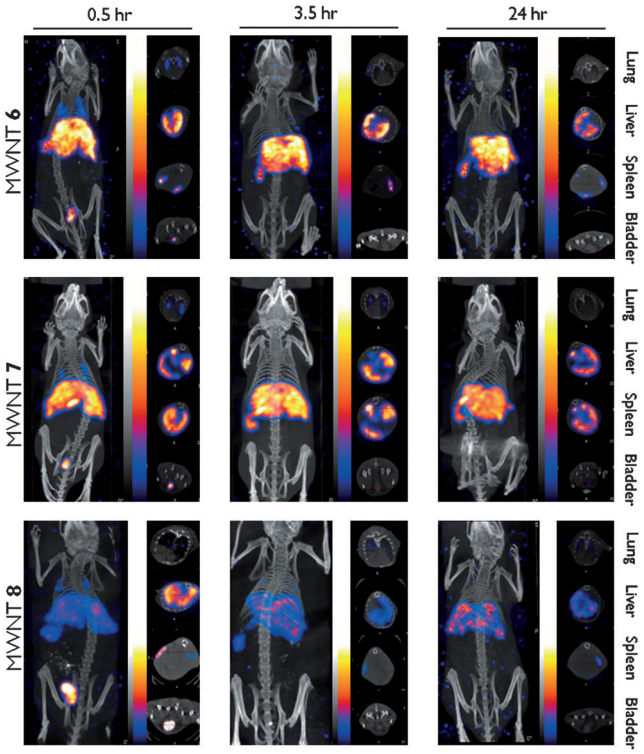

Figure 2. Whole-body imaging. Nano-SPECT/CT fused images of the whole mouse. Images were taken at 0.5, 3.5 and 24 h post-injection for MWNTs **6**, **7**, and **8** after injection of 50 μg of ^{111}In-DTPA-MWNTs with a scanning time up to 0.5 h.

bladder signals were more intense in MWNT **8** than MWNTs **6** and **7**. The percentage of the injected dose detected in the bladder, quantified by SPECT, at all time points are summarized in Table S3 (see Supporting Information). A higher degree of chemical functionalization led to enhanced renal clearance at 0.5 h. As expected, free ^{111}In-EDTA showed accumulation mainly in the kidneys and the bladder at 0.5 and 3.5 h, with no signal detected at all at 24 h (Supporting Information, Figure S4).

After 24 h, organs were removed to obtain an independent quantitative estimation of the percentage of the injected dose retained in major organs by gamma scintigraphy. Results were expressed as a percentage of the injected dose per gram tissue (%ID/g) and a percentage of the injected dose per organ (%ID/organ). In the case of MWNTs **6** and **7**, the highest %ID/g was detected in liver, spleen, and lung in the following order: liver > spleen > lung (Figure 3). This result agreed with the SPECT/CT imaging.

In the case of MWNT **8**, a reduction in liver accumulation (from 70–80% to less than 60%ID/g) and an increase in spleen and lung accumulation were measured compared to MWNTs **6** and **7**, confirming the SPECT imaging results. We also observed lung to spleen translocation of MWNTs **6** and **7** over time. A similar result was previously reported for pristine and ^{14}C-taurine-MWNTs, which could be explained by the translocation of overloaded MWNTs from the lungs to the afferent lymphatics and then to the spleen.[18,19] No difference in biodistribution profile was noted when DTPA was substituted with 1,4,7,10-tetraazacyclododecane-1,4,7,10-tetraacetic acid (DOTA) in MWNT **8** (Supporting Information, Figure S5). The percentage of the injected dose recovered from the major organs (liver, spleen, lung, and kidney) by gamma scintigraphy was 63.4%, 71.6%, and 49.0% for **6**, **7**, and **8**, respectively (see Supporting Information, Table S3).

To further analyze the pharmacokinetic data obtained in these experiments, experimentally determined values of ^{111}In concentration in the blood were fitted in bi-exponential function models (refer to Supporting Information for further details). The pharmacokinetic parameters determined are shown in Table 1. Immediately after injection, the percentage of the injected dose detected in the blood declined rapidly for all MWNTs (Figure 4). Two half-lives were calculated. The short first-phase half-life $t_{1/2\alpha}$ (ca. 0.013 h^{-1}–0.053 h^{-1}, Table 1) suggested that MWNTs were distributed rapidly between blood (central compartment) and tissues (peripheral compartment) with the possibility of rapid renal excretion taking place. After a pseudo-equilibrium distribution has been achieved, a second phase follows where blood levels of MWNTs **6**, **7**, and **8** very slowly declined.

Table 1: Blood half-life ($t_{1/2}$) and volume of distribution (V_d) after intravenous administration of *f*-MWNTs.

f-MWNTs	$t_{1/2\alpha}$ [h^{-1}][a]	$t_{1/2\beta}$ [h^{-1}][a]	V_d [mL][b]
MWNT **6**	0.019	0.96	3.995
MWNT **7**	0.053	3.10	5.219
MWNT **8**	0.013	7.03	1.904

[a] Obtained by fitting data points in a bi-exponential function model. [b] The fitted value at $t=0$ is given by $f_{(0)}=A+B$ and the corresponding volume of distribution factor is given by $V_d'=100/f_{(0)}=100/(A+B)$. A and B are the coefficients of the exponential terms (see Supporting Information for more details). The actual volume of distribution is then given by $V_d=V_d'\times 1.7$ mL, where we have assumed a blood volume of 1.7 mL for a 20 g mouse.

In this second phase, the reduction in plasma concentrations is primarily due to nanotube elimination, in contrast to the initial phase where the rapid reduction in plasma concentrations was also related to organ distribution.[20] The elimination half-life $t_{1/2\beta}$ was calculated and estimated to be in the range of about 0.96–7.03 h^{-1}. Despite the fact that all MWNTs had similar blood profiles, a closer inspection in the $t_{1/2\beta}$ suggested that MWNT **8** ($t_{1/2\beta}=7.03\ h^{-1}$) exhibited a longer elimination half-life compared to MWNTs **6** ($t_{1/2\beta}=0.96\ h^{-1}$) and **7** ($t_{1/2\beta}=3.1\ h^{-1}$). In contrast, at early time points (up to 0.1 h) MWNT **8** ($t_{1/2\alpha}=0.013\ h^{-1}$) decayed faster than MWNT **6** ($t_{1/2\alpha}=0.019\ h^{-1}$) and MWNT **7** ($t_{1/2\alpha}=0.053\ h^{-1}$), which further agrees with the rapid renal clearance detected by SPECT/CT imaging of MWNT **8**. Volume of distribution (V_d) was calculated by dividing the injected dose by the blood concentration at zero hours. High V_d values (approximately 1.9–4.0 mL; Table 1) were obtained and can be explained by a broad distribution of MWNT into major organs.

Long-term tissue distribution of non-radiolabeled MWNTs **8** was further assessed by histological examination of fixed and stained sections from major organs at 1 h, 7 days, and 30 days post-administration. Hematoxylin and eosin

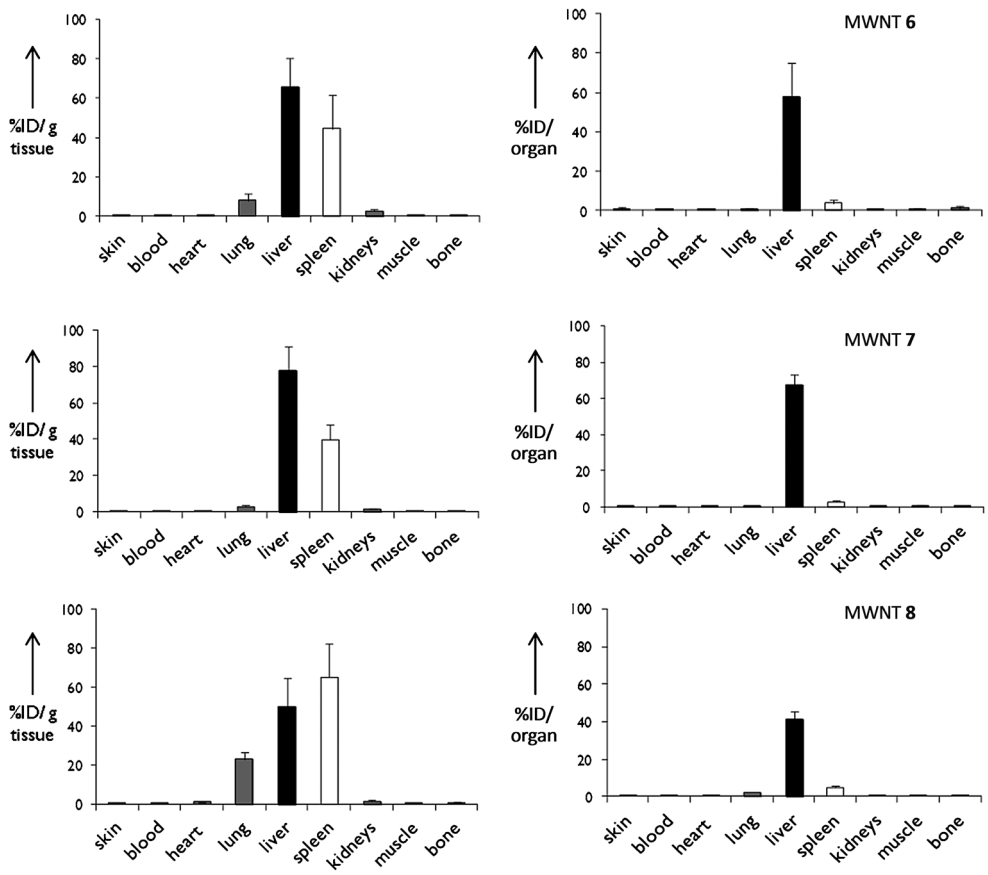

Figure 3. Quantitative tissue distribution. Results shown as a percentage of the injected dose per gram tissues (%ID/g) or per organ (%ID/organ) at 24 h after injection of 50 μg of ^{111}In-DTPA-MWNTs, quantified by gamma scintigraphy. Data are expressed as means ± SD (n = 3–4).

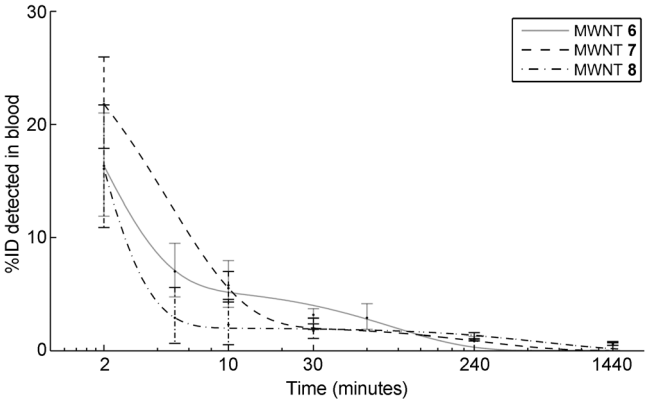

Figure 4. Pharmacokinetic modeling analysis. Blood-clearance profile of DTPA-MWNTs (mean ± SD, n = 3–4).

(H&E) stained sections revealed that there were no signs of tissue necrosis, fibrosis, or inflammation at all three time intervals (Supporting Information, Figure S6–S8). In neutral red-stained sections, MWNTs **8** appeared as black spots of varying size. Large and small clusters of MWNTs **8** were observed in the lung at 1 h and 7 days, but only large clusters remained in the lung after 30 days. Smaller clusters of MWNTs **8** were widely distributed throughout the liver and spleen at earlier time points but then were gradually reduced over the 30 day period. There was evidence of small, scattered CNT clusters in the kidney but this had reduced to a nominal level at 30 days (Supporting Information, Figure S6). This result confirmed the occurrence of a second (β) phase characterized by slow clearance of MWNTs **8** from major organs over a prolonged period of time, as predicted by kinetic modeling studies.

It has been reported that pristine SWNTs (not chemically functionalized) coated with the block co-polymer Pluronic F108 accumulated in the liver.[12] We also reported that serum-coated pristine MWNTs mainly resided in the liver and lung.[14] The rationale for hepatic accumulation was the desorption of physically adsorbed macromolecules upon entrance into the systemic blood compartment that can result in bundling of the nanotubes.[11] Accumulation of chemically functionalized CNTs in organs of the RES has also been reported, and the difference in hydrophobicity of the hydroxylated versus chelate/amine functionalized CNTs was thought to be responsible for the accumulation in the liver.[18] In this study, liver accumulation of the chemically functionalized DTPA-MWNTs can be attributed to possible in vivo bundling owing to insufficient surface functionalization. We and others have independently described that individualized, well-dispersed MWNTs were detected in the renal capillary lumen and during translocation through the glomerular filtration barrier with their longitudinal axis vertically oriented to the endothelial fenestrations.[10,21] We can conclude from such studies that differences in CNT individualization (i.e. how many nanotubes are isolated from one another) can determine their excretion profile in vivo, in which only individualized nanotubes of average diameter 20–30 nm can be excreted through the kidney. In this study, the diameter of all the constructs was in the range of the glomerular filtration cut off (ca. 30 nm). The results indicate that the difference in organ distribution and excretion profiles was mainly dependent on the degree of chemical functionalization, which is expected to directly affect CNT individualization. A fraction (greater than 17 % of the injected dose; Table S3) of MWNTs **8** escaped the glomerular filter, while the majority of aggregated nanotubes accumulated in the liver, spleen, and lung. These findings

have three implications: 1) they confirm that previous studies showing rapid renal clearance and low tissue retention were due to the individualization of CNTs, as a result of the high degree of chemical functionalization (over 0.99 mmol g^{-1});[7,8,10] 2) renal excretion is not only length-dependent as both MWNTs **7** and MWNTs **8** were shortened and of approximately the same dimensions, however MWNTs **8** showed improved renal clearance compared to MWNTs **7**; and 3) increasing the degree of chemical functionalization in a controlled manner can enhance renal clearance, while decreasing the degree of chemical functionalization will favor RES organ accumulation.

In conclusion, from this study we envisage that by tuning the degree of surface chemical functionalization of CNTs, greater control over their organ distribution and clearance profiles in vivo can be achieved. Controlling these properties is considered extremely important for the future design of CNT-based diagnostics and therapeutics.

Experimental Section

Multi-walled carbon nanotubes (MWNTs) were purchased from Nanostructured & Amorphous Materials Inc. (Houston). MWNTs used in this study were 94% pure (stock no. 1240XH). Their outer diameter was between 20 and 30 nm, and length was between 0.5 and 2 μm. For chemical functionalization of MWNTs **6**, MWNT-NH_3^+ **2** was made using a 1,3-dipolar cycloaddition reaction (loading: 0.058 mmol g^{-1} of amino functional groups) as reported.[6] After derivatization with DTPA, the MWNTs **6** were recovered by centrifugation, washed with water, and reprecipitated from MeOH/diethyl ether. The reaction went to completion, as confirmed by a negative Kaiser test. For chemical functionalization of MWNTs **7**, MWNTs **1** were first oxidized by acid treatment,[6] then treated with Boc-monoprotected diaminotriethyleneglycol (TEG) followed by a deprotection step to afford ammonium functionalized MWNTs (MWNT-TEG-NH_3^+; MWNTs **4**).[22] A Kaiser test confirmed amine loading of 0.115 mmol g^{-1}. MWNTs **4** were treated with DTPA, and a Kaiser test showed that 0.080 mmol g^{-1} of free ammonium groups were still present. To increase the amount of amino groups (MWNTs **5**) for the subsequent introduction of the chelating agent DTPA, the functionalization of oxidized nanotubes was repeated as for MWNTs **4** but the reaction conditions were slightly changed (see Supporting Information for further details). Kaiser tests confirmed a loading of 0.320 and 0.034 mmol g^{-1} of free amines before and after DTPA conjugation, respectively. Details of chemical functionalization of MWNTs **6**, **7**, and **8**, their radiolabeling and the pharmacokinetic modeling studies are fully described in the Supporting Information.

Received: March 13, 2012
Published online: May 23, 2012

Keywords: biodistribution · functionalization · nanotubes · pharmacokinetics · toxicology

[1] S. Iijima, *Nature* **1991**, *354*, 56–58.
[2] D. Tasis, N. Tagmatarchis, A. Bianco, M. Prato, *Chem. Rev.* **2006**, *106*, 1105–1136.
[3] V. Georgakilas, K. Kordatos, M. Prato, D. M. Guldi, M. Holzinger, A. Hirsch, *J. Am. Chem. Soc.* **2002**, *124*, 760–761.
[4] K. Kostarelos, L. Lacerda, G. Pastorin, W. Wu, S. Wieckowski, J. Luangsivilay, S. Godefroy, D. Pantarotto, J.-P. Briand, S. Muller, M. Prato, A. Bianco, *Nat. Nanotechnol.* **2007**, *2*, 108–113.
[5] S. Niyogi, M. A. Hamon, H. Hu, B. Zhao, P. Bhowmik, R. Sen, M. E. Itkis, R. C. Haddon, *Acc. Chem. Res.* **2002**, *35*, 1105–1113.
[6] V. Georgakilas, N. Tagmatarchis, D. Pantarotto, A. Bianco, J.-P. Briand, M. Prato, *Chem. Commun.* **2002**, 3050–3051.
[7] R. Singh, D. Pantarotto, L. Lacerda, G. Pastorin, C. Klumpp, M. Prato, A. Bianco, K. Kostarelos, *Proc. Natl. Acad. Sci. USA* **2006**, *103*, 3357–3362.
[8] L. Lacerda, A. Soundararajan, R. Singh, G. Pastorin, K. T. Al-Jamal, J. Turton, P. Frederik, M. A. Herrero, S. L. A. Bao, D. Emfietzoglou, S. Mather, W. T. Phillips, M. Prato, A. Bianco, B. Goins, K. Kostarelos, *Adv. Mater.* **2008**, *20*, 225–230.
[9] J. Wang, X. Y. Deng, S. T. Yang, H. F. Wang, Y. L. Zhao, Y. F. Liu, *Nanotoxicology* **2008**, *2*, 28–32.
[10] A. Ruggiero, C. H. Villa, E. Bander, D. A. Rey, M. Bergkvist, C. A. Batt, K. Manova-Todorova, W. M. Deen, D. A. Scheinberg, M. R. McDevitt, *Proc. Natl. Acad. Sci. USA* **2010**, *107*, 12369–12374.
[11] J. Guo, X. Zhang, Q. Li, W. Li, *Nucl. Med. Biol.* **2007**, *34*, 579–583.
[12] P. Cherukuri, C. J. Gannon, T. K. Leeuw, H. K. Schmidt, R. E. Smalley, S. A. Curley, R. B. Weisman, *Proc. Natl. Acad. Sci. USA* **2006**, *103*, 18882–18886.
[13] Z. Liu, C. Davis, W. B. Cai, L. He, X. Y. Chen, H. J. Dai, *Proc. Natl. Acad. Sci. USA* **2008**, *105*, 1410–1415.
[14] L. Lacerda, H. Ali-Boucetta, M. A. Herrero, G. Pastorin, A. Bianco, M. Prato, K. Kostarelos, *Nanomedicine* **2008**, *3*, 149–161.
[15] K. Kostarelos, *Nat. Mater.* **2010**, *9*, 793–795.
[16] S. Li, W. Wu, S. Campidelli, V. Sarnatskaïa, M. Prato, A. Tridon, A. Nikolaev, V. Nikolaev, A. Bianco, E. Snezhkova, *Carbon* **2008**, *46*, 1091–1095.
[17] F. Jasanada, P. Urizzi, J. P. Souchard, G. F. Le, G. Favre, F. Nepveu, *Bioconjugate Chem.* **1996**, *7*, 72–81.
[18] X. Deng, G. Jia, H. Wang, H. Sun, X. Wang, S. Yang, T. Wang, Y. Liu, *Carbon* **2007**, *45*, 1419–1424.
[19] S. T. Yang, W. Guo, Y. Lin, X. Y. Deng, H. F. Wang, H. F. Sun, Y. F. Liu, X. Wang, W. Wang, M. Chen, Y. P. Huang, Y. P. Sun, *J. Phys. Chem. C* **2007**, *111*, 17761–17764.
[20] P. L. Toutain, A. Bousquet-Melou, *J. Vet. Pharmacol. Ther.* **2004**, *27*, 427–439.
[21] L. Lacerda, M. A. Herrero, K. Venner, A. Bianco, M. Prato, K. Kostarelos, *Small* **2008**, *4*, 1130–1132.
[22] W. Wu, S. Wieckowski, G. Pastorin, M. Benincasa, C. Klumpp, J. P. Briand, R. Gennaro, M. Prato, A. Bianco, *Angew. Chem.* **2005**, *117*, 6516–6520; *Angew. Chem. Int. Ed.* **2005**, *44*, 6358–6362.

